Numerical modeling of waves incident on slip discontinuities

Matthew Haney and Roel Snieder
Center for Wave Phenomena, Colorado School of Mines, Golden, CO 80401

ABSTRACT
Interfaces in elastic media need not be in welded contact. For instance, fractures allow a small amount of slip to occur along their surfaces during the passage of a seismic wave. By slip, we mean that the displacement across the interface can be discontinuous. Reflection and transmission of plane waves in this case are frequency dependent.
Previous numerical studies have chosen the finite-difference method to simulate slip discontinuities. The approach suffers from difficulties in incorporating boundary conditions into the strong form of the equations of motion. We show in detail that only a finite-element formulation of the σ-v (stress and velocity) equations can overcome these problems. Numerical examples illustrate the method for an SH-wave normally incident on a slip discontinuity and a P-wave incident at an angle.

1 INTRODUCTION

Full-waveform forward modeling in seismology has traditionally been dominated by finite-difference methods. Perhaps the intuitive appeal of such methods has led to their popularity. Kelly and Marfurt (1990), in reviewing the numerical literature from the exploration geophysics community, cited at least four possible reasons for the relative neglect of other methods, specifically finite-elements. We complement their list by stating that finite-elements require additional numerical detail to implement properly. For instance, explicit finite-difference algorithms do not require the inversion of a matrix. In contrast, all finite-element methods eventually lead to a matrix equation that must be solved.

Finite-elements offer more flexibility than finite-differences with respect to the shape of the numerical mesh; however, it is less widely accepted that finite-elements are superior to finite-differences in the way they account for boundary conditions. Such an advantage can easily be seen in the formula for integration by parts: an integral is replaced by another integral *and* a term representing the values of the function at the boundaries. This basic fact shows up in the formulation of finite-elements since they approximate the integrated, or weak, equations of motion.

Finite-differences, as approximations to the strong form of the equations of motion, require ad hoc techniques to take into account, for instance, a welded boundary between two different elastic media. David Boore, one of the pioneers of the finite-difference method in seismology, summarized the problem by stating that in finite-difference schemes "the interface displacements must satisfy the continuity of displacement and stress, but are not explicitly required to satisfy the equation of motion" (Boore, 1970).

The motivation of this paper is to explore the advantages of the finite-element method for the modeling of slip discontinuities. The slip discontinuity has been proposed by Schoenberg (1980) as an interface condition applicable to cracks. The boundary condition can be thought of as a generalized interface condition since it supplies a parameter, the compliance η, that, over its range of physical values, takes an elastic interface from a welded contact ($\eta = 0$) to a free surface ($\eta = \infty$). Mathematically, a slip discontinuity for an SH-wave is expressed as

$$u_y^+ - u_y^- = \eta \sigma_{yz}, \tag{1}$$

$$\sigma_{yz}^+ - \sigma_{yz}^- = 0, \tag{2}$$

where (-) refers to the side of the interface on which the wave is incident, (+) the other side of the interface, u_y refers to the displacement normal to the plane of propagation, and σ_{yz} is the shear stress. In this paper, a slip discontinuity extends infinitely; we do not consider crack-tips. Physically, boundary conditions (1) and (2) model the transmission and reflection of a thin, low shear zone (Schoenberg, 1980). Faults generally fall within this category.

In this paper, we will argue three main points:

1. Finite-element modeling is needed to incorporate interface boundary conditions into the equations of motion.
2. The equations of motion should be the first-order σ-v (stress and velocity) system of partial differential equations instead of the second-order wave equation in u (displacement) to avoid any finite-difference-like approximations to spatial derivatives.
3. Only an implicit, unconditionally stable time integration scheme can handle the zero-length elements needed to accurately model a slip discontinuity.

We conclude this discussion of the finite-element method with numerical examples of the reflection and transmission of plane SH- and P-waves at a slip discontinuity.

2 A FINITE-ELEMENT SCHEME FOR THE 1D SCALAR WAVE EQUATION

The beginning of any numerical study must be an analysis of the two competing limitations imposed on finite systems: numerical dispersion and stability. An understanding of these concepts should steer the subsequent implementation of a particular numerical scheme. Ideally, any numerical simulation should satisfy a stability criterion with the least amount of dispersion possible.

In this section, we present the most simple case: a finite-element implementation of the scalar wave equation in 1D. We choose this problem since, in 1D, the essence of the finite-element scheme is not complicated by mesh generation or subsequent "assembly" of the mass or stiffness matrix. Assembly of these matrices is directly related to the notion of wrapping up, or ordering, a higher-dimensional set of points into a 1D vector. In 1D, this is not necessary.

We consider the 1D scalar wave equation with source term in a homogeneous medium

$$c^2\frac{\partial^2 u}{\partial z^2} - \frac{\partial^2 u}{\partial t^2} - s = 0, \tag{3}$$

and assume Dirichlet (essential) boundary conditions at $z = 0$ and $z = L$. The displacement, u, is approximated by a finite series of spatial basis functions with coefficients that depend on time

$$u(z,t) = \sum_{K=1}^{N} \alpha_K(t)\phi_K(z). \tag{4}$$

In this paper, the nodal basis will always be used. For a spatial discretization step h and a uniform partition of the interval $[0,L]$ into $N+1$ subintervals, these basis functions are mathematically defined as

$$\phi_K(z) = \begin{cases} (z - z_{K-1})/h & \text{if } z_{K-1} \le z \le z_K, \\ (z_{K+1} - z)/h & \text{if } z_K \le z \le z_{K+1}, \\ 0 & \text{otherwise.} \end{cases} \tag{5}$$

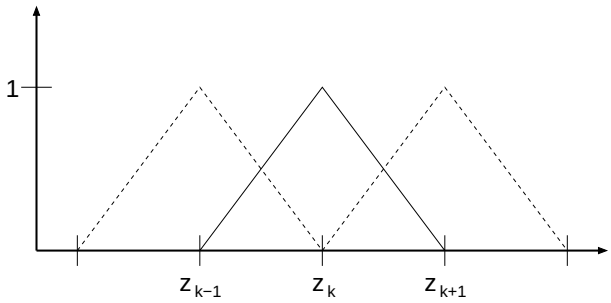

Figure 1. The basis functions we use for finite-elements.

Fig. 1 shows these piecewise linear functions graphically.

The Galerkin formulation of the finite-element method seeks to minimize the weighted average of the error induced by the incompleteness of the finite set of basis functions in equation (5) The essence of the Galerkin method is that it weights the errors with the same basis functions used in the approximation of the displacement, u (Marfurt, 1984)

$$\int_0^L \left[c^2\frac{\partial^2}{\partial z^2}\sum_{K=1}^{N}\alpha_K(t)\phi_K(z) - \frac{\partial^2}{\partial t^2}\sum_{K=1}^{N}\alpha_K(t)\phi_K(z) - s \right]\phi_J(z)dz = 0$$
$$\text{for } J=1,2,...,N. \tag{6}$$

Rearranging the order of the sums and integrals in this equation yields

$$0 = -c^2\sum_{K=1}^{N}\alpha_K\left[\int_0^L \frac{\partial^2\phi_K}{\partial z^2}\phi_J dz\right] + \sum_{K=1}^{N}\frac{\partial^2\alpha_K}{\partial t^2}\left[\int_0^L \phi_K\phi_J dz\right] + \int_0^L s\phi_J dz. \tag{7}$$

Since the basis functions are piecewise linear over their range, the first integral on the r.h.s. of equation (7), containing a second derivative of the basis function, must be altered (Haltiner and Williams, 1980). It turns out that in altering this term by integrating by parts, boundary terms appear explicitly in the equation of motion

$$\int_0^L \frac{\partial^2\phi_K}{\partial z^2}\phi_J dz = \left.\frac{\partial\phi_K}{\partial z}\phi_J\right|_0^L - \int_0^L \frac{\partial\phi_K}{\partial z}\frac{\partial\phi_J}{\partial z}dz. \tag{8}$$

To implement Dirichlet boundary conditions at $z = 0$ and $z = L$, the weighting function, ϕ_J, is set to zero at the boundaries (Wang, 2000). Hence, the boundary term in equation (8) disappears and the elements ϕ are fixed to be zero on the boundaries. More complicated boundary conditions, such as absorbing boundary conditions, are not discussed here.

Without the boundary term, inserting equation (8)

into equation (7) yields the weak form of the scalar wave equation

$$0 = c^2 \sum_{K=1}^{N} \alpha_K \left[\int_0^L \frac{\partial \phi_K}{\partial z} \frac{\partial \phi_J}{\partial z} dz \right] + \sum_{K=1}^{N} \frac{\partial^2 \alpha_K}{\partial t^2} \left[\int_0^L \phi_K \phi_J dz \right] + \int_0^L s \phi_J dz. \quad (9)$$

The bracketed terms in equation (9) can be represented as matrices multiplying the vectors $\vec{\alpha}$ and $\ddot{\vec{\alpha}}$. The matrix multiplying the second time derivative, $\ddot{\vec{\alpha}}$, is usually called the *mass matrix*, M, and the matrix acting on $\vec{\alpha}$ is referred to as the *stiffness matrix*, S. From equation (5), the entries of these matrices can be calculated exactly. For the mass matrix, $M_{K,J}$, the non-zero entries are

$$\int_0^L \phi_K \phi_J dz = 2h/3 \qquad \text{for } K = J \quad (10)$$

$$\int_0^L \phi_K \phi_J dz = h/6 \qquad \text{for } K = J+1, J-1. \quad (11)$$

This means that M is symmetric and tridiagonal. Similarly, the stiffness matrix, $S_{K,J}$, is also symmetric tridiagonal and the non-zero entries are

$$\int_0^L \frac{\partial \phi_K}{\partial z} \frac{\partial \phi_J}{\partial z} dz = 2/h \qquad \text{for } K = J \quad (12)$$

$$\int_0^L \frac{\partial \phi_K}{\partial z} \frac{\partial \phi_J}{\partial z} dz = -1/h \qquad \text{for } K = J+1, J-1. \quad (13)$$

The finite-element scheme can now be written in matrix form

$$0 = c^2 S \vec{\alpha} + M \ddot{\vec{\alpha}}. \quad (14)$$

Note that the source term has been omitted in equation (14). In our numerical simulations, we use an initial condition as a source instead of a forcing term in the equations of motion. To include a forcing term, s has to be approximated in the nodal basis

$$s(z,t) = \sum_{K=1}^{N} s_K(t) \phi_K(z). \quad (15)$$

Substituting this into equation (9), it can be seen that the mass matrix multiplies the source vector.

3 STABILITY ANALYSIS OF AN EXPLICIT FINITE-ELEMENT SCHEME

The finite-element approach has served to integrate the above matrix equation in space, but a suitable time integration scheme has yet to be determined. As a first example, we use an explicit time integration known as central differences (Zienkiewicz and Taylor, 2000) to approximate the time behavior of $\vec{\alpha}$

$$0 = c^2 S \vec{\alpha}_n + M \left(\frac{\vec{\alpha}_{n+1} - 2\vec{\alpha}_n + \vec{\alpha}_{n-1}}{\Delta t^2} \right) \quad (16)$$

where the subscripts refer to the time step $n+1$, to be calculated, and the previous time steps n and $n-1$. The time discretization interval is shown as Δt. Notice that equation (16) is symmetric in the $n+1$ and $n-1$ terms. This ensures that the resulting dispersion relation on the numerical grid is real-valued. Such a property is desirable since a complex dispersion relation would yield solutions to the wave equation that grow or decay exponentially with distance. In contrast, real-valued solutions do not grow exponentially, so long as they satisfy a stability criterion.

To calculate the stability criterion of this explicit time integration scheme, first use equations (10), (11), (12), and (13) to carry out the matrix multiplications in equation (16). What results is the so-called *finite-element stencil*

$$\begin{aligned} 0 \;=\; & \frac{h}{6\Delta t^2}\alpha_{m-1,n+1} + \frac{2h}{3\Delta t^2}\alpha_{m,n+1} + \\ & \frac{h}{6\Delta t^2}\alpha_{m+1,n+1} - \left(\frac{h}{3\Delta t^2} + \frac{c^2}{h}\right)\alpha_{m-1,n} - \\ & \left(\frac{4h}{3\Delta t^2} - \frac{2c^2}{h}\right)\alpha_{m,n} - \left(\frac{h}{3\Delta t^2} + \frac{c^2}{h}\right)\alpha_{m+1,n} + \\ & \frac{h}{6\Delta t^2}\alpha_{m-1,n-1} + \frac{2h}{3\Delta t^2}\alpha_{m-1,n-1} + \\ & \frac{h}{6\Delta t^2}\alpha_{m-1,n-1}, \end{aligned} \quad (17)$$

where the first subscripts refer to gridpoints in space and the second subscripts are still the time steps. To investigate the stability of the central difference scheme, insert a harmonic function for α (Alterman and Loewenthal, 1970)

$$\alpha_{m,n} = e^{ikmh}\zeta^n \quad \zeta = e^{b\Delta t},\ z = mh, \text{ and } t = n\Delta t, \quad (18)$$

where the integers m and n multiply the spatial and temporal interval lengths h and Δt, and k is the wavenumber.

Inserting equation (18) into equation (17), and organizing terms yields

$$\begin{aligned} 0 \;=\; & \left[\frac{h}{6\Delta t^2}(e^{-ikh} + 4 + e^{ikh})\zeta^2 \right. \\ & -\frac{c^2}{h}(e^{-ikh} - 2 + e^{ikh})\zeta \\ & -\frac{h}{3\Delta t^2}(e^{-ikh} + 4 + e^{ikh})\zeta \\ & \left. +\frac{h}{6\Delta t^2}(e^{-ikh} + 4 + e^{ikh}) \right] e^{ikmh}\zeta^{n-1}. \end{aligned} \quad (19)$$

In order to have non-trivial solutions, the terms inside the brackets in equation (19) must equal zero. The resulting equation contains all the information about

the dispersion and stability properties of the numerical scheme. Note that in higher dimensions, equation (19) is a matrix equation and the condition for non-trivial solutions is that the determinant of the matrix equals zero.

Dividing equation (19) by the coefficient of the ζ^2 term and setting the terms inside the brackets to zero gives

$$0 = \zeta^2 - \frac{6c^2\Delta t^2}{h^2}\left(\frac{e^{-ikh} - 2 + e^{ikh}}{e^{-ikh} + 4 + e^{ikh}}\right)\zeta - 2\zeta + 1. \quad (20)$$

Using the Euler formula and the relation $\cos(kh) - 1 = -2\sin^2(kh/2)$, we can simplify equation (20)

$$0 = \zeta^2 - \left[\frac{\frac{2h}{\Delta t^2} - \left(\frac{4c^2}{h} + \frac{4h}{3\Delta t^2}\right)\sin^2(kh/2)}{\frac{h}{\Delta t^2} - \frac{2h}{3\Delta t^2}\sin^2(kh/2)}\right]\zeta + 1. \quad (21)$$

For the numerical scheme to be stable, the roots of equation (21) should have magnitudes less than or equal to 1. This means that the solutions are not exponentially growing in time. For a quadratic of the form

$$0 = x^2 - zx + 1, \quad (22)$$

the magnitude of the two roots, x_1 and x_2, are both less than or equal to 1 if

$$-1 \leq \frac{z}{2} \leq 1. \quad (23)$$

Inserting equation (21) into this expression yields

$$-1 \leq \frac{\frac{2h}{\Delta t^2} - \left(\frac{4c^2}{h} + \frac{4h}{3\Delta t^2}\right)\sin^2(kh/2)}{2(\frac{h}{\Delta t^2} - \frac{2h}{3\Delta t^2}\sin^2(kh/2))} \leq 1. \quad (24)$$

Scanning over all possible values of $\sin^2(kh/2)$, the strongest condition on the spatial and temporal discretizations h and Δt occurs when $\sin^2(kh/2) = 1$ (Alterman and Loewenthal, 1970). In this case, equation (24) becomes:

$$-1 \leq \frac{\frac{2h}{3\Delta t^2} - \frac{4c^2}{h}}{\frac{2h}{3\Delta t^2}} \leq 1. \quad (25)$$

From equation (25), the right inequality:

$$\frac{2h}{3\Delta t^2} - \frac{4c^2}{h} \leq \frac{2h}{3\Delta t^2}, \quad (26)$$

is trivially true. The left inequality provides a more meaningful relation:

$$\begin{aligned} -\frac{2h}{3\Delta t^2} &\leq \frac{2h}{3\Delta t^2} - \frac{4c^2}{h}, \\ \frac{4c^2}{h} &\leq \frac{4h}{3\Delta t^2}, \\ c\Delta t\sqrt{3} &\leq h. \end{aligned} \quad (27)$$

This is the Courant-Friedrichs-Levy (CFL) stability condition for this implementation of explicit finite elements (Marfurt, 1984).

Above, we stated that equation (19) contains all the information about the dispersion and stability properties of the numerical scheme. We have the stability condition - what about the dispersion relation? To obtain this, set b in equation (18) to $i\omega$ so that $\zeta = e^{i\omega\Delta t}$. Substituting this into equation (19), setting the terms in the brackets to zero, and simplifying a bit yields the dispersion relation

$$\cos(\omega\Delta t) = 1 + \frac{3\Delta t^2 c^2}{h^2}\left(\frac{\cos(kh) - 1}{\cos(kh) + 2}\right). \quad (28)$$

For wavelengths much larger than the grid-spacing, $\omega\Delta t$ and kh are small parameters. Keeping the lowest order terms in a series expansion of equation (28) gives the well-known relation

$$\omega^2 = c^2k^2. \quad (29)$$

In other words, the finite-element scheme should do an excellent job propagating waves well-sampled by the numerical grid.

4 ZERO-LENGTH ELEMENTS FOR FRACTURES

The finite-element example explored above shows the essence of the numerical implementation of the weak form of the equations of motion. It is relatively easy to code since all that is needed is the inversion of a tridiagonal matrix. Modeling interfaces in elastic media, though, introduces several complications.

To model true boundaries, some of the elements should have zero length. In this way, two points on opposite sides of a crack, but infinitesimally close to one another, could be modeled precisely. Explicit finite-elements of the second-order wave equation fail this requirement for two reasons. First, entries in the stiffness matrix, equations (12) and (13), go to infinity as h goes to zero. Second, even if the stiffness matrix existed, the CFL-condition, equation (27), would demand that the time discretization Δt go to zero if the length of any element went to zero. This statement assumes that the CFL-condition acts at each point in the computational domain for an irregular grid (which has been verified numerically).

In addition, the boundary conditions in elastic media concern the continuity or relationship of displacement and stress at an interface. Discrete approximations of the stress would have to do for an implementation of the wave equation in displacement. By formulating a finite-element analysis for the σ-v (stress and velocity) system of equations, the stress would be available in the numerical scheme without approximation. Furthermore, it turns out that the mass and stiffness matrices in the σ-v formulation can accommodate elements of zero length. The next section will explore this in more detail.

The solution to the problem of the CFL condition

for an element of zero length is to use an implicit time integration scheme that is *unconditionally* stable. To illustrate unconditional stability, consider this alternative time scheme for equation (16)

$$0 = c^2 S\left(\frac{\vec{\alpha}_{n+1}+\vec{\alpha}_{n-1}}{2}\right) + M\left(\frac{\vec{\alpha}_{n+1}-2\vec{\alpha}_n+\vec{\alpha}_{n-1}}{\Delta t^2}\right), \quad (30)$$

where now the value of α at the time n is replaced by a simple average of its values at times $n+1$ and $n-1$. Note again that this expression is symmetric in the terms at $n+1$ and $n-1$ so that the dispersion relation is real-valued. By going through the same steps outlined previously to obtain the stability of this time integration scheme (which we call *forward-backward time integration*), the CFL-like condition that results is

$$-2h^2 \leq 3c^2\Delta t^2, \quad (31)$$

which is always true. Hence, the forward-backward time scheme is unconditionally stable. This sort of time scheme makes the modeling of zero-length elements possible.

5 A FINITE-ELEMENT SCHEME FOR STRESS-VELOCITY IN 1D

In 1D, all three elastic wave types decouple since they are normally incident on interfaces. Here, we focus the analysis to the SH-wave. The system of partial differential equations for velocity and stress in this case is

$$\frac{\partial v_y}{\partial t} - \frac{1}{\rho}\frac{\partial \sigma_{yz}}{\partial z} = 0, \quad (32)$$

$$\frac{\partial \sigma_{yz}}{\partial t} - \mu\frac{\partial v_y}{\partial z} = 0. \quad (33)$$

These equations are recognized as Newton's and Hooke's Laws, respectively. The same nodal basis as above is used to approximate the velocity and stress

$$v_y(z,t) = \sum_{K=1}^{N} \alpha_K(t)\phi_K(z), \quad (34)$$

$$\sigma_{yz}(z,t) = \sum_{K=1}^{N} \beta_K(t)\phi_K(z), \quad (35)$$

and Dirichlet boundary conditions are assumed to apply on the ends of some domain $z = 0$ to $z = L$. Applying the Galerkin method to equation (32), as was done to the scalar wave equation, and integrating by parts gives the resulting weak form

$$\sum_{K=1}^{N} \frac{\partial \alpha_K}{\partial t}\left[\int_0^L \phi_K\phi_J dz\right] = -\frac{1}{\rho}\sum_{K=1}^{N}\beta_K\left[\int_0^L \phi_K\frac{\partial\phi_J}{\partial z}dz\right]. \quad (36)$$

In this equation, the mass matrix (multiplying $\dot{\vec{\alpha}}$) is identical to the one for the scalar wave equation; however, the "stiffness" matrix (multiplying $\vec{\beta}$) has a different form. Using equation (5), the entries of this new stiffness matrix, $S_{K,J}$, can be calculated

$$\int_0^L \phi_K\frac{\partial\phi_J}{\partial z}dz = -1/2 \qquad \text{for } K = J+1 \quad (37)$$

$$\int_0^L \phi_K\frac{\partial\phi_J}{\partial z}dz = 1/2 \qquad \text{for } K = J-1. \quad (38)$$

The matrix form of equation (36) is thus

$$M\dot{\vec{\alpha}} = -\frac{1}{\rho}S\vec{\beta}. \quad (39)$$

Note that the entries of this stiffness matrix are constants, independent of the spatial discretization h. This is in contrast to the expression for the second-order wave equation. The independence of this stiffness matrix from h allows zero length elements to be modeled in the finite-element implementation of the σ-v system.

For the second equation in the σ-v system, equation (33), we apply the Galerkin method but stop short of integrating by parts

$$\sum_{K=1}^{N} \frac{\partial \beta_K}{\partial t}\left[\int_0^L \phi_K\phi_J dz\right] = \mu\sum_{K=1}^{N}\alpha_K\left[\int_0^L \frac{\partial\phi_K}{\partial z}\phi_J dz\right]. \quad (40)$$

The term on the l.h.s. of equation (40) is similar to what has been encountered up to this point. The new challenge is to properly treat the first term on the r.h.s., since it contains information about slip discontinuities. That is the subject of the next section.

6 THE INCLUSION OF A SLIP DISCONTINUITY

The first step in evaluating the term on the r.h.s. of equation (40) involves breaking the integral into two - one running up to the fault (or fracture), and the other continuing on the other side of the fault. In the limit of

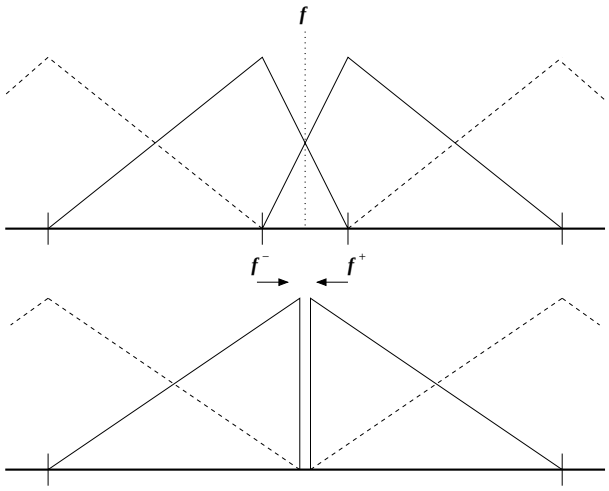

Figure 2. The limiting procedure we use in creating a slip discontinuity. The fault, f, is placed between two nodes whose positions eventually coincide with each other.

the fault having no thickness (a slip discontinuity)

$$\mu \sum_{K=1}^{N} \alpha_K \left[\int_0^L \frac{\partial \phi_K}{\partial z} \phi_J dz \right] =$$
$$\mu \sum_{K=1}^{N} \alpha_K \left[\int_0^{f^-} \frac{\partial \phi_K}{\partial z} \phi_J dz + \int_{f^+}^{L} \frac{\partial \phi_K}{\partial z} \phi_J dz \right]. \quad (41)$$

After integrating by parts and combining the resulting two integrals back into a single integral from $z = 0$ to $z = L$, we obtain for the r.h.s. of equation (41)

$$\mu \sum_{K=1}^{N} \alpha_K \left[\phi_K \phi_J |_0^{f^-} + \phi_K \phi_J |_{f^+}^{L} - \int_0^L \phi_K \frac{\partial \phi_J}{\partial z} dz \right]. \quad (42)$$

For simplicity at this point, assume Dirichlet boundaries at $z = 0$ and $z = L$, and distribute the sums

$$\mu \sum_{K=1}^{N} \alpha_K \left(\phi_K(f^-)\phi_J(f^-) - \phi_K(f^+)\phi_J(f^+) \right) -$$
$$\mu \sum_{K=1}^{N} \alpha_K \int_0^L \phi_K \frac{\partial \phi_J}{\partial z} dz. \quad (43)$$

The term with the integral is ready to go into the equations of motion. Notice that it has the same stiffness matrix as in equation (36). The other term represents the slip discontinuity explicitly. To evaluate this term, we first place the nodes of our basis functions at f^- and f^+, (Fig. 2). The weighting functions ϕ_J in equation (43) are continuous at the fault, and we set them to their values at the nodes f^- and f^+ (unity). We then take the limit as $f^- \to f^+$, creating a zero-length element at the fault. The leftmost term of equation (43) becomes

$$-\mu \sum_{K=1}^{N} \alpha_K \left(\phi_K(f^+) - \phi_K(f^-) \right). \quad (44)$$

The series in this equation is the slip in the nodal basis. Taking the time-derivative of equation (1), we replace the terms inside the series with the nodal basis representation of the time-derivative of the stress at the fault multiplied by the compliance, η

$$-\mu\eta \frac{\partial}{\partial t} \sum_{K=1}^{N} \beta_K \phi_K(f), \quad (45)$$

where f is located halfway between f^- and f^+ (see Fig. 2). Since we have put two nodes centered at f^- and f^+, the ϕ_K in equation (45) are all zero except for the two that straddle the fault. When evaluated at f, both of these nodal basis functions are equal to 1/2, making the previous equation a simple average

$$-\frac{\mu\eta}{2} \frac{\partial}{\partial t} \left(\beta^{f^-} + \beta^{f^+} \right), \quad (46)$$

where the superscripts f^- and f^+ denote that these terms are non-zero for only the two nodes nearest the fault. In taking the limit as the fault thickness goes to zero, these two nodes represent displacement and stress infinitely close to, but on opposite sides of, a slip discontinuity.

Substituting equation (46) into equations (43) and (40), we obtain the weak form of the second equation in the σ-v system

$$\sum_{K=1}^{N} \frac{\partial \beta_K}{\partial t} \left[\int_0^L \phi_K \phi_J dz \right] = -\frac{\mu\eta}{2} \frac{\partial}{\partial t} \left(\beta^{f^-} + \beta^{f^+} \right)$$
$$-\mu \sum_{K=1}^{N} \alpha_K \int_0^L \phi_K \frac{\partial \phi_J}{\partial z} dz. \quad (47)$$

Putting this equation into matrix notation using the mass and stiffness matrices, the finite-element system in the σ-v formulation is

$$M\dot{\vec{\alpha}} = -\frac{1}{\rho} S\vec{\beta}, \quad (48)$$

$$M\dot{\vec{\beta}} = -\mu S\vec{\alpha} - \frac{\mu\eta}{2} \frac{\partial}{\partial t} \left(\beta^{f^-} + \beta^{f^+} \right). \quad (49)$$

7 A NUMERICAL EXAMPLE IN 1D

In implementing equations (48) and (49), we chose an implicit time integration scheme so that zero-length elements at the slip discontinuity could be modeled without stability issues. Denoting the values of displacement

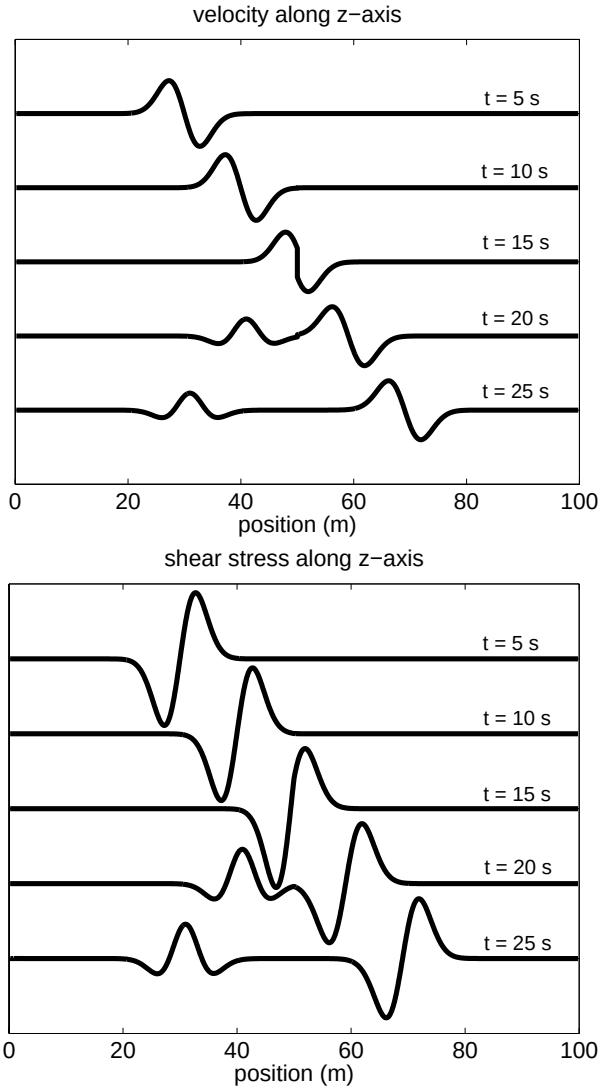

Figure 3. Snapshots of the velocity and stress fields at five different times. There is a slip discontinuity at z = 50 m.

and stress at a future timestep by $n+1$ and at previous timesteps as n and $n-1$, the system of equations is

$$M\frac{\vec{\alpha}_{n+1}-\vec{\alpha}_{n-1}}{2\Delta t} = -\frac{1}{\rho}S\frac{\vec{\beta}_{n+1}+\vec{\beta}_{n-1}}{2}, \tag{50}$$

$$M\frac{\vec{\beta}_{n+1}-\vec{\beta}_{n-1}}{2\Delta t} = -\mu S\frac{\vec{\alpha}_{n+1}+\vec{\alpha}_{n-1}}{2} + -\frac{\mu\eta}{2}\frac{\beta^{f^-}_{n+1}-\beta^{f^-}_{n-1}}{2\Delta t} - \frac{\mu\eta}{2}\frac{\beta^{f^+}_{n+1}-\beta^{f^+}_{n-1}}{2\Delta t}. \tag{51}$$

This system of equations is solved in Matlab using LU decomposition to obtain the values of stress and displacement at time $n+1$. Note that no additional constraints to account for boundary conditions are needed - the boundary conditions are integrated in equations (50) and (51).

Figure 3 shows the velocity and stress, calculated from equations (50) and (51), at several moments in time. The simulation had an initial condition representing a plane wave incident from the left. At the center, $z = 50$ m, is a slip discontinuity with compliance η equal to .5 $\mathrm{s}^2\mathrm{m}^2/\mathrm{kg}$. The media are identical on either side of the slip discontinuity. For a compliance of zero, the two media would be in welded contact and there would be no reflection. The wave reflected from the slip discontinuity is the derivative of the incident wave, as pointed out by Widess (1973), and hence has a higher frequency content. The slip discontinuity is actually an infinitesimally thin bed; in the parlance of scattering theory, it is a 1D Rayleigh point scatterer.

Assuming a high velocity thin bed, Widess concluded that the reflection of the thin bed would become negligible for a bed thickness less than one-eighth of a wavelength (Widess, 1973). So why is it that the slip discontinuity simulated here gave such a strongly reflected wave? From Schoenberg (1980), we know that a slip discontinuity models the reflection from a thin, low shear layer. For a sufficiently low shear velocity, there is no lower limit to the thickness of a bed that would produce a significant S-wave reflection. Extremely low shear wave velocities have been observed in laboratory measurements of fluid pressurized sands (Zimmer *et al.*, 2002) and can be expected to occur in "blown" faults that have high pore pressures in the fault itself. Hence, the slip discontinuity should be an excellent model for a "blown" fault.

Note that the stress is continuous and the velocity *discontinuous* across the imperfect interface. This has been accomplished with the zero-length elements at the slip discontinuity. Figure 4 shows detail of the wavefield near the fracture. Plotted along the horizontal axis is the position. The zero length element shows up as a kink in the stress and a velocity jump in this plot. We have benchmarked the results of the numerical simulation with the analytic expressions for reflection and transmission coefficients at a slip discontinuity (Schoenberg, 1980; Pyrak-Nolte *et. al*, 1990). We obtain excellent agreement over the frequency band used in the simulation.

8 EXTENSION TO THE P-SV CASE IN 2D

Of more interest to seismic surveys is the reflection and transmission of $P-SV$-waves at a slip discontinuity. Two compliances, the normal and tangential compliances (η_N and η_T), characterize a crack in this case. Analogous to equations (1) and (2), the interface boundary conditions are

$$u_x^+ - u_x^- = \eta_T\sigma_{xz}, \tag{52}$$

$$\sigma_{xz}^+ - \sigma_{xz}^- = 0, \tag{53}$$

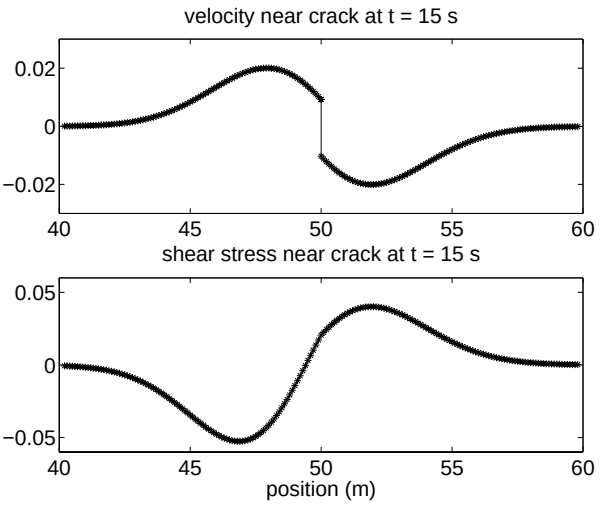

Figure 4. Detail of the velocity and stress fields near the crack at 15 s. The discontinuity is easily seen in the velocity at the crack, whereas the stress is continuous.

$$u_z^+ - u_z^- = \eta_N \sigma_{zz}, \tag{54}$$

$$\sigma_{zz}^+ - \sigma_{zz}^- = 0. \tag{55}$$

In what follows, we assume that $\eta_N = 0$, *i.e.* the crack is a thin low shear zone, but not a zone of low bulk modulus.

The equations of motion for $P-SV$-waves couple two components of displacement with three stresses

$$\frac{\partial v_x}{\partial t} - \frac{1}{\rho}\left[\frac{\partial \sigma_{xx}}{\partial x} + \frac{\partial \sigma_{xz}}{\partial z}\right] = 0, \tag{56}$$

$$\frac{\partial \sigma_{xz}}{\partial t} - \mu\left[\frac{\partial v_x}{\partial z} + \frac{\partial v_z}{\partial x}\right] = 0, \tag{57}$$

$$\frac{\partial v_z}{\partial t} - \frac{1}{\rho}\left[\frac{\partial \sigma_{xz}}{\partial x} + \frac{\partial \sigma_{zz}}{\partial z}\right] = 0, \tag{58}$$

$$\frac{\partial \sigma_{zz}}{\partial t} - \lambda\frac{\partial v_x}{\partial x} - (\lambda+2\mu)\frac{\partial v_z}{\partial z} = 0, \tag{59}$$

$$\frac{\partial \sigma_{xx}}{\partial t} - (\lambda+2\mu)\frac{\partial v_x}{\partial x} - \lambda\frac{\partial v_z}{\partial z} = 0. \tag{60}$$

Since the quantity σ_{xx} does not enter into the boundary conditions, it makes sense to eliminate it from this system of equations. To do so, we use the fact that, in a medium with 1D variation with depth (a $c(z)$ medium), the horizontal component of the slowness

$$p_x = \frac{sin\theta}{c}, \tag{61}$$

for the incident angle θ from the vertical and medium velocity c, is constant. Symbolically, this means that plane wave solutions for any of the displacements or stresses in a $c(z)$ medium would have the form $S(t - p_x x - p_z z)$. The horizontal slowness, p_x, does not change when the background velocity changes. With this information

$$\frac{\partial \sigma_{xx}}{\partial t} = -\frac{1}{p_x}\frac{\partial \sigma_{xx}}{\partial x}, \tag{62}$$

$$\frac{\partial v_x}{\partial x} = -p_x\frac{\partial v_x}{\partial t}, \tag{63}$$

and substituting this into equation (60) yields

$$\frac{\partial \sigma_{xx}}{\partial x} - p_x^2(\lambda+2\mu)\frac{\partial v_x}{\partial t} - p_x\lambda\frac{\partial v_z}{\partial z} = 0. \tag{64}$$

Equation (64) can be used to eliminate σ_{xx} in equation (56). Notice that we have also replaced a derivative w.r.t. x with a t-derivative in equation (63). Using this same trick on equations (57)-(59), $P-SV$ propagation in a $c(z)$ medium can be written as a system of 4 PDEs with derivatives in t and z only

$$\frac{\partial v_x}{\partial t}(1 - p_x^2 V_p^2) - \frac{1}{\rho}\frac{\partial \sigma_{xz}}{\partial z} + p_x\frac{\lambda}{\rho}\frac{\partial v_z}{\partial z} = 0, \tag{65}$$

$$\frac{\partial \sigma_{xz}}{\partial t} - \mu\frac{\partial v_x}{\partial z} + p_x\mu\frac{\partial v_z}{\partial t} = 0, \tag{66}$$

$$\frac{\partial v_z}{\partial t} - \frac{1}{\rho}\frac{\partial \sigma_{zz}}{\partial z} + p_x\frac{1}{\rho}\frac{\partial \sigma_{xz}}{\partial t} = 0, \tag{67}$$

$$\frac{\partial \sigma_{zz}}{\partial t} - (\lambda+2\mu)\frac{\partial v_z}{\partial z} + p_x\lambda\frac{\partial v_x}{\partial t} = 0, \tag{68}$$

where $V_p = \sqrt{(\lambda+2\mu)/\rho}$ is the velocity of the P-wave. Note that for normal incidence ($p_x = 0$), the system of 4 PDEs decouples into 2 systems of 2 PDEs in the form of equations (32) and (33).

Applying the same Galerkin method to equations (65)-(68), we use the expansions

$$v_x(z,t) = \sum_{K=1}^{N} \alpha_K(t)\phi_K(z), \tag{69}$$

$$\sigma_{xz}(z,t) = \sum_{K=1}^{N} \beta_K(t)\phi_K(z), \tag{70}$$

$$v_z(z,t) = \sum_{K=1}^{N} \gamma_K(t)\phi_K(z), \tag{71}$$

$$\sigma_{zz}(z,t) = \sum_{K=1}^{N} \delta_K(t)\phi_K(z). \tag{72}$$

Including a slip discontinuity from equations (52) and (53), the matrix equations are

$$(1 - p_x^2 V_p^2)M\frac{\vec{\alpha}_{n+1} - \vec{\alpha}_{n-1}}{2\Delta t} = -\frac{1}{\rho}S\frac{\vec{\beta}_{n+1} + \vec{\beta}_{n-1}}{2} + \frac{\lambda}{\rho}p_x S\frac{\vec{\gamma}_{n+1} + \vec{\gamma}_{n-1}}{2}, \tag{73}$$

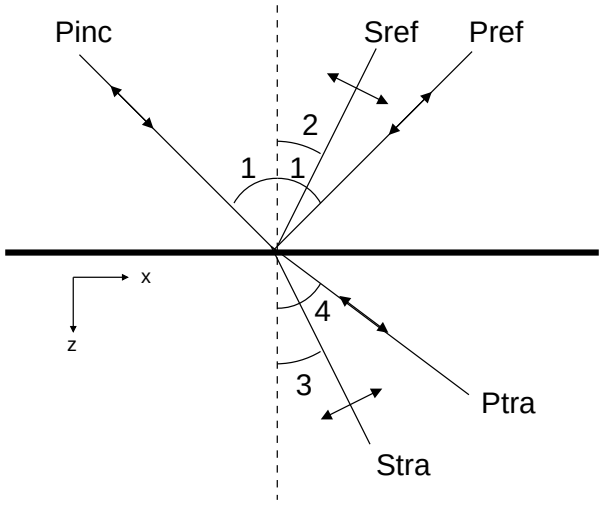

Figure 5. A P-wave is incident at an angle of 45° with the vertical on a horizontal slip discontinuity. Four waves radiate from the imperfect interface. The compliance of the crack does not affect the directions of the reflected, transmitted, and converted waves, only their magnitudes and frequency content.

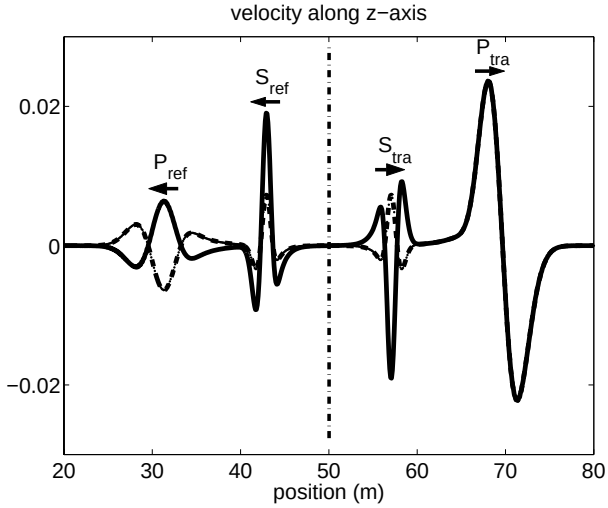

Figure 6. Snapshot of the vertical and horizontal velocity fields after the incident P-wave has interacted with a slip discontinuity. The vertical velocity is shown as a solid line, with the horizontal velocity a dashed line. The slip discontinuity is at z = 50 m, marked by a vertical dashed-dot line. The incident wave is a P-wave incident at an angle of 45° with the vertical.

$$M\frac{\vec{\beta}_{n+1}-\vec{\beta}_{n-1}}{2\Delta t}=-\mu S\frac{\vec{\alpha}_{n+1}+\vec{\alpha}_{n-1}}{2}$$
$$-p_x\mu M\frac{\vec{\gamma}_{n+1}-\vec{\gamma}_{n-1}}{2\Delta t}$$
$$-\mu\eta_T\frac{\beta^{f^-}_{n+1}-\beta^{f^-}_{n-1}}{2\Delta t}-\mu\eta_T\frac{\beta^{f^+}_{n+1}-\beta^{f^+}_{n-1}}{2\Delta t}, \qquad (74)$$

$$M\frac{\vec{\gamma}_{n+1}-\vec{\gamma}_{n-1}}{2\Delta t}=-\frac{1}{\rho}S\frac{\vec{\delta}_{n+1}+\vec{\delta}_{n-1}}{2}$$
$$-\frac{1}{\rho}p_xM\frac{\vec{\beta}_{n+1}-\vec{\beta}_{n-1}}{2\Delta t}, \qquad (75)$$

$$M\frac{\vec{\delta}_{n+1}-\vec{\delta}_{n-1}}{2\Delta t}=-(\lambda+2\mu)S\frac{\vec{\gamma}_{n+1}+\vec{\gamma}_{n-1}}{2}$$
$$-p_x\lambda M\frac{\vec{\alpha}_{n+1}-\vec{\alpha}_{n-1}}{2\Delta t}. \qquad (76)$$

These equations are implicit expressions for the time step $n+1$ and can be solved by LU decomposition for the components $[\vec{\alpha}_{n+1},\vec{\beta}_{n+1},\vec{\gamma}_{n+1},\vec{\delta}_{n+1}]$.

We show an example where the simulation for the $P-SV$ case is initialized with an incident P-wave at an angle of 45°. Depicted in Fig. 5 are the directions of the reflected and transmitted waves. In specifying initial conditions, the wavelet for the vertical and horizontal velocities, w, had to be projected into the vertical direction, and the waveforms for the 2 stress components were computed from Hooke's Law.

A result of the numerical $P-SV$ simulation is shown in Fig. 6. The tangential compliance, η_T, equals .5 $\mathrm{s^2m^2/kg}$, as in the previous example. Since the slip discontinuity is between two identical media, the incident P-wave should not change direction. To check that the numerical simulation preserved the incident direction, note how the vertical and horizontal velocities overlap for the transmitted P-wave in Fig. 6. This overlap occurs for the propagation angle 45°, the same as the incident P-wave. Also shown in Fig. 6 are the converted waves S_{ref} and S_{tra}. They have a higher frequency content than the incident wave and the signs of their components determine their respective polarizations. These polarizations agree with the S-waves expected from Fig. 5.

9 CONCLUSIONS

The exercise of realizing slip discontinuities in a simple 1D finite-element algorithm should assist in the implementation of slip interfaces in 2D numerical codes, which are further complicated by meshing and assembly issues. We find that proper modeling of fractures demands an implicit, unconditionally stable time integration scheme. Future work should explore if an explicit time scheme is at all possible, since this would increase the computational efficiency needed for an extension to a 2D or 3D code. In 2D or 3D, the repeated use we made of integration by parts in this paper would be replaced by Green's Theorem. Simulations in a higher dimension would allow the modeling of crack tips.

In the numerical examples, we kept the background medium homogeneous except for the slip discontinuities. The finite-element scheme can also be worked out in the

case of smoothly-varying changes in the material properties. An example of this would be a zone of linearly increasing velocity bounded by two slip discontinuities. A zero-length element is also necessary in simulating a welded interface.

We limited our study to the reflection and transmission of a pure slip (displacement) discontinuity. Schoenberg (1980) has also suggested the possibility of a viscous slip condition. Other, more exotic interface conditions exist, such as the Maxwell and Kelvin versions of the combined displacement and velocity discontinuity (Pyrak-Nolte, 1996). This interface condition models the reflection and transmission from a thin, low shear zone with attenuation and has been validated in laboratory experiments (Pyrak-Nolte *et. al*, 1990). The same finite-element methods we have described here are needed to numerically model these other types of interfaces.

ACKNOWLEDGMENTS

We would like to thank Yaping Zhu and Jon Sheiman for discussions on fault zones. Shell has generously provided funding for this work.

REFERENCES

Alterman, Z. S., and Loewenthal, D. 1970. Seismic Waves in a Quarter and Three-Quarter Plane, *Geophys. J. R. astr. Soc.*, **20**, *101*.

Boore, D. M. 1970. Finite difference solutions to the equations of elastic wave propagation, with applications to Love waves over dipping interfaces, *Ph.D. thesis, Massachusetts Institute of Technology*.

Coates, R. T., and Schoenberg, M. 1995. Finite-difference modeling of faults and fractures, *Geophysics*, **60**, *1514*.

Haltiner, G. J., and Williams, R. T. 1980. *Numerical Prediction and Dynamic Meteorology*, Wiley, New York.

Kelly, K. R., Ward, R. W., Treitel, S., and Alford, R. M. 1976. Synthetic seismograms: A finite-difference approach, *Geophysics*, **41**, *2*.

Kelly, K. R., and Marfurt, K. J., eds. 1990. *Numerical Modeling of Seismic Wave Propagation*, SEG Geophysics reprint series No. 13.

Lysmer, J., and Drake, L. A. 1972. A finite element method for seismology, in: *Methods in computational physics v.11*, ed. B. A. Bolt, Academic Press, New York.

Marfurt, K. J. 1984. Accuracy of finite-difference and finite-element modeling of the scalar and elastic wave equations. *Geophysics*, **49**, *533*.

Pyrak-Nolte, L., Myer, L., and Cook, N. 1990. Transmission of Seismic Waves Across Single Natural Fractures, *JGR*, **95**, *8617*.

Pyrak-Nolte, L. 1996. The seismic response of fractures and the interrelations among fracture properties, *Int. Journ. of Rock Mechanics and Mining Sci. and Geomech. Abstr.*, **8**, *785*.

Schoenberg, M. 1980. Elastic wave behavior across linear slip interfaces, *J. Acoust. Soc. Am.*, **68**, *1516*.

Shampine, L. F., Allen, Jr., R. C., and Pruess, S. 1997. *Fundamentals of Numerical Computing*, Wiley, New York.

Smith, W. 1975. The Application of Finite Element Analysis to Body Wave Propagation Problems, *Geophys. J. R. astr. Soc.*, **42**, *747*.

Wang, J. 2000. Finite Element Methods: Theory and Implementation, *Course Notes, Colorado School of Mines*.

Widess, M. B. 1973. How Thin is a Thin Bed? *Geophysics*, **38**, *1176*.

Zhu, Y., and Snieder, R. 2002. Reflected and transmitted waves from fault zones, *SEG Int'l Exposition and 72nd Annual Meeting, Salt lake City, Utah*, *2273*.

Zienkiewicz, O. C., and Taylor, R. L. 2000. *The Finite Element Method, v.1*, Butterworth-Heinemann, Oxford.

Zimmer, M., Prasad, M., and Mavko, G. 2002. Pressure and porosity influences on $V_P - V_S$ ratio in unconsolidated sands. *The Leading Edge*, **21**, *178*.